

and the Université d'Antananarivo in 1995. Etymology: *Rahona* (RAH-hoo-nah; Malagasy): meaning menace/threat or cloud; intended interpretation: "menace from the clouds"; *ostromi*: in honor of Dr. John H. Ostrom. Diagnosis: *Rahona ostromi* is distinguished from all other avians by retention of a robust, hyperextendible, pedal digit II; from all other avians except *Patagonykus* by hyposphene-hypantra articulations on dorsal vertebrae; from *Archaeopteryx* by six fused sacral vertebrae and a greatly reduced fibula lacking contact with the calcaneum; from nonavian theropods, *Archaeopteryx*, and alvarezsaurids by its relatively elongate ulna with ulnar papillae and mobile scapulocoracoid articulation; from all other avians except *Archaeopteryx* and alvarezsaurids by retention of a long tail lacking a pygostyle; and from nonavian theropods by neural canals at least 40% of the height of the dorsal vertebral centra, proximal tibia of equal width and length, lack of a medial fossa on the fibula, and a reversed pedal digit I.

14. C. A. Forster *et al.*, *Nature* **382**, 532 (1996).

15. The placement of *Patagonykus* and other alvarezsaurids (*Mononykus* and *Alvarezsaurus*) within Aves, although supported by cladistic analyses [for example, see (5, 6) and this analysis], is questioned by other researchers (10). Elimination of Alvarezsauridae from the phylogenetic analyses presented in this report does not alter the placement of *Rahona* within Aves.

16. B. Stephan, *Urvögel Archaeopterygiformes* (Ziemen, Wittenberg, Germany, 1974); S. Rietschel, in *The Beginnings of Birds*, M. K. Hecht, J. H. Ostrom, G. Viohl, P. Wellnhofer, Eds. (Brönnner and Daentler, Eichstätt, Germany, 1984), pp. 251–260.

17. F. A. Jenkins, *Am. J. Sci.* **293-A**, 253 (1993); S. A. Poore, A. Sánchez-Haiman, G. E. Goslow Jr., *Nature* **387**, 799 (1997).

18. F. E. Novas and P. F. Puerta, *Nature* **387**, 390 (1997).

19. J. H. Ostrom, *Peabody Mus. Bull.* **30**, 1 (1969).

20. P. J. Currie, *J. Vertebr. Paleontol.* **7**, 72 (1987); P. J. Currie and X. Zhao, *Can. J. Earth Sci.* **30**, 2231 (1993).

21. Morphological information from *Rahona* was combined with that of six bird and eight maniraptoran taxa into a 113-character matrix and analyzed with the PAUP and MacClade programs. Characters were unordered and unweighted, and trees were optimized with the use of delayed transformations. Tree statistics are as follows: The most parsimonious tree shown in Fig. 5A is 228 steps; consistency index (CI) = 0.579, homoplasy index (HI) = 0.421, retention index (RI) = 0.712. The tree shown in Fig. 5B is 229 steps; CI = 0.576, HI = 0.424, RI = 0.709. The character matrix and character list for this phylogenetic analysis are available at www.sciencemag.org/feature/data/972697.shl.

22. The three forelimb elements of *Rahona* were found either next to or touching the hind portion of the skeleton (Fig. 1B). Because they were not in direct articulation with the rear of the animal, we recognize the possibility, albeit remote in our opinion, that they do not belong to the same individual or taxon. Although material of more derived avians was found elsewhere in the quarry, with the exception of one articulated partial tibiotarsus-tarsometatarsus (14) all avian material occurred as widely scattered, isolated elements. The only articulated skeleton found anywhere in the quarry is that of *Rahona*. Because of the taphonomic distribution of bone in the quarry and the juxtaposition of these forelimb elements with the rear portion of the skeleton, we believe they belong to the same specimen and are confident in assigning them to *Rahona*. Nevertheless, to test the effect of an erroneous association, the phylogenetic analysis was run with two data sets, one including and one excluding forelimb elements for *Rahona*. Each data set resulted in two most parsimonious trees; the ambiguity in these trees was due to the switching of the positions of the theropod taxa Oviraptoridae and Ornithomimidae. The topology of taxa within Aves was consistent across all four most parsimonious trees, with *Rahona* firmly nested within this clade.

23. J. H. Ostrom, *The Beginnings of Birds*, M. K. Hecht, J. H. Ostrom, G. Viohl, P. Wellnhofer, Eds. (Brönnner and Daentler, Eichstätt, Germany, 1984), pp. 161–176; L. Hou, L. D. Martin, Z. Zhou, A. Feduccia, *Science* **274**, 1164 (1996); N. Bonde, in *The Continental Jurassic*, M. Morales, Ed. (Museum of Northern Arizona, Flagstaff, AZ, 1996), pp. 193–199.

24. It cannot be ascertained whether *Archaeopteryx* possesses hyposphene-hypantra articulations. Among more derived birds, only the alvarezsaurid *Patagonykus* retains this character.

25. The foot of *Unenlagia* is not known. However, it has been suggested that *Archaeopteryx* retains vestiges of an enlarged, hyperextendible, second pedal digit and claw. This observation was first advanced by J. Gauthier (3) and more recently revived by G. Paul [Programs and Abstracts, Society of Avian Paleontology and Evolution (Washington, DC, 1996), p. 15].

26. We thank B. Rakotosamimanana, P. Wright, B. Andriamihaja, the staff of the Institute for the Conservation of Tropical Environments, the people of Berivotra, and all expedition members for their help; and L. Witmer, J. Clark, and an anonymous reviewer for discussions and critiques. D. Varricchio, J. Clark, M. Norell, H. Osmólska, and P. Wellnhofer provided valuable information on theropods and *Archaeopteryx*. *Rahona* was prepared by V. Heisey and photographed by M. Stewart and F. E. Grine (with a scanning electron microscope), and figures were drawn by L. Betti-Nash and C.A.F. This work was supported by grants from NSF and The Dinosaur Society (to C.A.F., S.D.S., and D.W.K.) and the J. S. Guggenheim Foundation and F. Chapman Memorial Fund (to L.M.C.).

9 January 1998; accepted 5 February 1998

Age and Origin of Carlsbad Cavern and Related Caves from ⁴⁰Ar/³⁹Ar of Alunite

Victor J. Polyak,* William C. McIntosh,* Necip Güven, Paula Provencio

⁴⁰Ar/³⁹Ar dating of fine-grained alunite that formed during cave genesis provides ages of formation for the Big Room level of Carlsbad Cavern [4.0 to 3.9 million years ago (Ma)], the upper level of Lechuguilla Cave (6.0 to 5.7 Ma), and three other hypogene caves (11.3 to 6.0 Ma) in the Guadalupe Mountains of New Mexico. Alunite ages increase and are strongly correlative with cave elevations, which indicates an 1100-meter decline in the water table, apparently related to tectonic uplift and tilting, from 11.3 Ma to the present. ⁴⁰Ar/³⁹Ar dating studies of the hypogene caves have the potential to help resolve late Cenozoic climatic, speleologic, and tectonic questions.

Carlsbad Cavern and Lechuguilla Cave are world renowned for their size, geology, and mineral decorations. These and other related caves are located in the Permian Capitan Limestone, Goat Seep Dolomite, and associated backreef carbonate rocks in the Guadalupe Mountains of southeastern New Mexico and West Texas (1) (Fig. 1). Carlsbad, Lechuguilla, and other major caves of the Guadalupe Mountains formed partly, if not largely, by sulfuric acid dissolution (2–4) rather than solely by carbonic acid dissolution as was initially thought (5). Caves formed by ascending hydrothermal or sulfuric acid-bearing waters are termed hypogene (6–8). Hypogene caves represent at least 10% of the 300+ (9) caves in the Guadalupe Mountains; these are generally the larger caves. Some hypogene caves in the Carlsbad area contain small amounts of alunite, a potassium-bearing aluminum sulfate, which is a by-product of cave genesis (10). Alunite has been used for K-Ar and

⁴⁰Ar/³⁹Ar dating of hypogene and supergene hydrothermal ore deposits (11) and supergene paleoweathering sequences (12). Here, we use alunite to determine the absolute age of formation of Carlsbad Cavern and other related hypogene caves. Previously, ages of these (13) or any other dissolution caves could be estimated only by dating detrital sediments and carbonate precipitates, which establish only the earliest ages of calcite or clastic deposition in the caves.

Alunite is present in Carlsbad Cavern and related caves in floor deposits and wall residues and most commonly within pockets of altered bedrock or solution cavity fillings (10), which may represent paleokarst cavities. Alunite and hydrated halloysite are products of the reaction of acidic cave-forming waters with clays such as montmorillonite, illite, dickite, and kaolinite that occur as detrital components of cavity fillings or in scarce thin Permian clay beds. The Green Clay Room in Carlsbad Cavern presents the most convincing evidence of alteration by sulfuric acid of green montmorillonite-rich sediments that fill solution cavities; white reaction rims around these cavity fillings consist of alunite and hydrated halloysite (Fig. 2A). In Endless Cave, pods of white alunite and hydrated halloysite at the base of a 10-cm-thick Permian clay bed also provide

V. J. Polyak and N. Güven, Department of Geosciences, Texas Tech University, Lubbock, TX 79409–1053, USA. W. C. McIntosh, New Mexico Geochronology Research Laboratory, New Mexico Institute of Mining and Technology, Socorro, NM 87801–4796, USA. P. Provencio, Sandia National Laboratories, Albuquerque, NM 87185, USA.

*To whom correspondence should be addressed. E-mail: aqvjp@ttuvm1.ttu.edu and mcintosh@nmt.edu

good evidence that alunite and hydrated halloysite have formed from the kaolinite and illite-smectite mixed-layer clay that make up the clay bed (Fig. 2B). During cave genesis, K^+ and Al^{3+} from alteration of the clays combined with SO_4^{2-} to form alunite, $KAl_3(SO_4)_2(OH)_6$, which then began to accumulate ^{40}Ar from radioactive decay of ^{40}K . Because the alunite is a by-product of cave genesis, alunite ages represent the absolute ages of formation of these hypogene caves. Alunite, like the gypsum that formed during cave genesis (8), is found only in cave areas that have been protected from flood, seepage, and drip waters since the caves formed. Alunite crystals are euhedral and generally range from 1 to 5 μm across (Fig. 2C), although one sample contained crystals as large as 20 μm . We purified and separated alunite crystals by settling in water, yielding separates with as little as 3% adhering clay, mostly halloysite. Some samples were leached with hydrofluoric acid (HF) to re-

move all adhering clay.

$^{40}Ar/^{39}Ar$ age determinations of alunite separates were conducted by stepwise heating in a resistance furnace (14). Pertinent data are summarized in Table 1. Complete data tables are available online (14). The most precise ages, in millions of years (Ma), were obtained from HF-leached samples, which produced high yields of radiogenic ^{40}Ar (50 to 87%), high K/Ca ratios (77 to 676; calculated from $^{37}Ar_{Ca}/^{39}Ar_K$ ratios), and flat age spectra (Fig. 3). Plateau ages from the HF-treated samples range from 11.30 ± 0.17 Ma (Virgin Cave) to 3.89 ± 0.13 Ma (Green Clay Room, Carlsbad Cavern). Non-HF-treated samples with 1 to 5% halloysite contamination produced relatively flat age spectra with plateau ages as much as 5% older than correlative HF-leached samples (Fig. 4). Samples with larger amounts of clay contamination (10 to 50% halloysite and smectite) yielded disturbed age spectra with significantly elevated ages

and reduced radiogenic ^{40}Ar yields and K/Ca ratios (Fig. 4). In addition, the Permian clay bed in Endless Cave yielded an integrated $^{40}Ar/^{39}Ar$ age of 278 ± 3 Ma, illustrating that small amounts of contaminant clay greatly elevate the apparent age of alunite samples. Other potential problems with $^{40}Ar/^{39}Ar$ dating of very fine-grained mineral phases, such as the 1 to 20 μm alunite we examined, include reactor-induced recoil of ^{39}Ar (15) and loss, gain, or exchange of K or ^{40}Ar (16) at some time after initial crystallization of the alunite. Evidence that recoil effects are negligible, in accord with another study (17), includes the lack of a systematic relationship between age and K-derived ^{39}Ar and close similarity in apparent age among fractions of alunite crystals of various sizes (1.5 to 8.3 μm in diameter) separated from one sample (Table 1) (14). Furthermore, the flat nature of the pure alunite age spectra (Fig. 3) and agreement in age among multiple samples from the same locality and from similar elevations (Table 1) (14) suggest that significant exchange of K or Ar isotopes did not occur in the cave environment or during neutron irradiation.

Alunite ages for Carlsbad Cavern and related caves increase with cave elevation

Fig. 1. Map and profile of the Guadalupe Mountains of New Mexico and Texas. Numerous faults that have uplifted the block of carbonate rocks that make up the Guadalupe Mountains are north-northwest trending normal faults and define the western edge of the mountains (border fault zone in vicinity of Brokeoff Mountains) (1). The Capitan reef is exposed along the southeastern escarpment. Guadalupe Peak is the highest point in the mountains. Profile A-A' shows the general stratigraphy of the Permian rocks, location of four caves, and position of the present water table from Lechuguilla Cave to the city of Carlsbad.

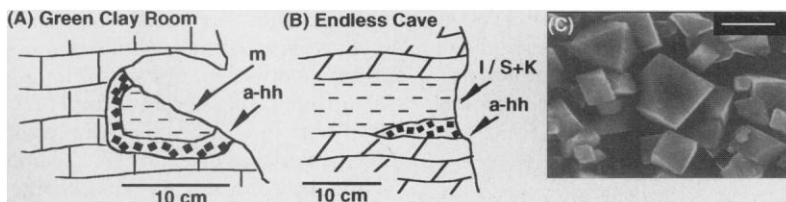
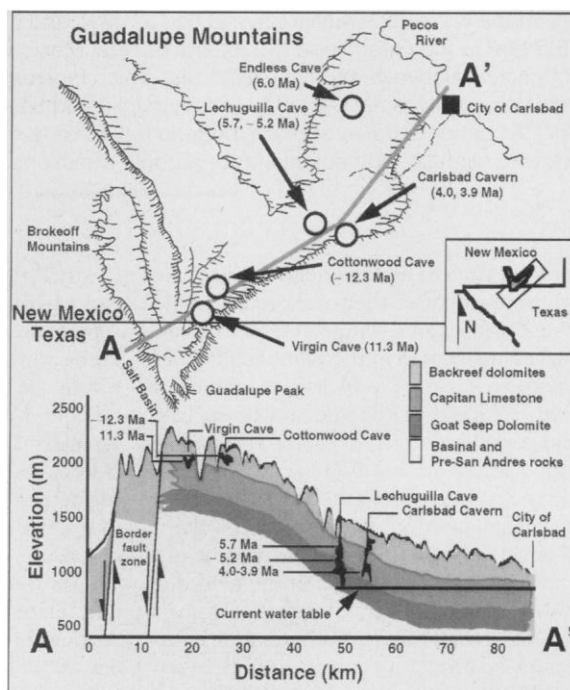


Fig. 2. Two examples of cave settings showing the physical relationships between wall rock and alunite and an image of alunite crystals. (A) Green montmorillonite-rich sediment (m) filling solution cavities has been truncated by sulfuric acid-related cave genesis and altered to alunite and hydrated halloysite (a-hh). (B) Brown Permian clay bed of illite-smectite mixed layers and kaolinite has been truncated by cave genesis and altered to a-hh. (C) Scanning electron micrograph showing typical euhedral rhombs of fine-grained cave alunite. Bar = 3 μm .

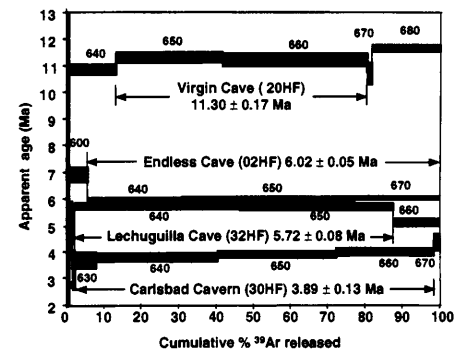


Fig. 3. $^{40}Ar/^{39}Ar$ age spectra and plateau ages from pure, HF-treated alunite samples.

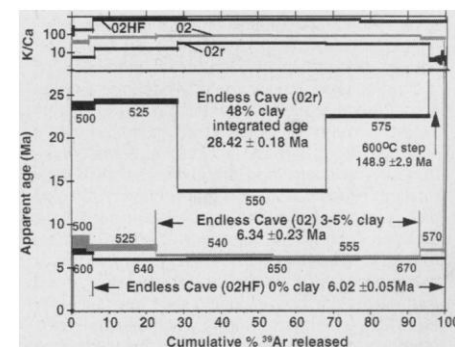


Fig. 4. $^{40}Ar/^{39}Ar$ age spectra of alunite samples from Endless Cave, illustrating elevated apparent ages caused by different contents of contaminant clay.

and fall into two distinct groups (Fig. 5). The two main dated periods of cave formation are 12 to 11 Ma for Cottonwood Cave and Virgin Cave at elevations of 2040 to 2010 m and 6 to 4 Ma for Lechuguilla Cave, Endless Cave, and Carlsbad Cavern (1230 to 1090 m). There are few known hypogene caves in the Carlsbad area at elevations of 1500 to 1750 m. There are many known hypogene caves at elevations of 1250 to 1500 and 1750 to 2010 m, but these have not been found to contain alunite. Within Carlsbad Cavern, samples from the edge and center of the Big Room yielded analytically identical ages of 4.07 ± 0.07 and 4.00 ± 0.04 Ma. Alunite from the New Mexico Room and the Green Clay Room, located at the same elevation interval (1135 to 1090 m), have comparable ages (3.98 ± 0.13 and 3.89 ± 0.13 Ma). Glacier Bay in Lechuguilla Cave (1230 m) and Endless Cave (1250 m) are separated by 25 km but contain alunite with closely comparable ages (5.72 ± 0.08 Ma and 6.02 ± 0.05 Ma). In addition, a Lechuguilla Cave sample from Lake LeBarge at an elevation of 1180 m (between the elevations of Glacier

Bay and the Big Room) yielded an age of 5.16 ± 0.13 Ma. All of the $^{40}\text{Ar}/^{39}\text{Ar}$ ages are significantly older than the previously reported late Pliocene to Pleistocene (1.2 to 0.75 Ma) minimum age of formation for the lower levels of Carlsbad Cavern (13).

The formation of caves in the Carlsbad area between 12 and 4 Ma was apparently influenced by tectonic and climatic control of the position of the water table in the permeable Capitan Limestone aquifer (18) and flow of hydrogen sulfide-bearing waters from the adjacent Delaware Basin. Hydrogen sulfide migrated upward along the base of the impermeable anhydrite of the Castile Formation in the basin. The caves apparently formed where the migrating hydrogen sulfide met the water table in the Capitan aquifer (4, 8, 9). Cottonwood Cave, Virgin Cave, and other caves began to form 12 to 11 Ma near the border faults along the western edge of the mountains near Guadalupe Peak. Between 12 and 4 Ma, cave formation shifted progressively toward the east-northeast as the water table in the Capitan Limestone dropped, probably as a result of uplift of the Guadalupe block. Erosion of the Castile anhydrite was concurrent with uplift (or water table decline). Eventually, exposure of the more resistant Capitan reef limestone as an escarpment disrupted the hydrogen sulfide pathway (4, 9). Cave elevations indicate that, between 12 Ma and the present, the water table in the Capitan Limestone dropped 1100 m, which coincides closely with the estimated 1200-m maximum vertical fault displacement of the Guadalupe block (1). Currently active sulfuric acid-driven dissolution has not been reported in any of the known caves, although it is

possibly occurring in the Capitan Limestone at lower elevations to the east of the Guadalupe Mountains where sulfur-bearing water has been reported in cavernous porosity (9). At present, the elevation of the water table in the Carlsbad Cavern area is 950 m (18).

The Neogene episodes of cave genesis are coeval with a period of regional basin and range and Rio Grande rift extension and associated volcanism (9, 19) and with global climatic fluctuations linked to development of deep weathering sequences (20). The specific locations of major hypogene caves were probably influenced by locations of joints and mild folds in the Capitan Limestone. Less well known are the factors that affected the episodic nature of the timing of cave genesis and the extent of dissolution and therefore size of the caves. Higher rates of fresh groundwater flow through the Capitan aquifer may have provided more oxidative conditions favorable for the production of sulfuric acid and extensive removal of dissolved carbonates. The bimodal distribution of elevation of the larger (hypogene) caves may reflect periods of increased precipitation around 12 to 11 and 6 to 4 Ma.

Age determinations of hypogene caves are important because nearly 10% of known major caves worldwide are hypogene in origin (7). Many of these are sulfuric acid caves that contain alunite. We envision that studies and age determinations of hypogene caves worldwide will contribute valuable information about late Cenozoic geologic and climatic history.

REFERENCES AND NOTES

1. P. B. King, *U.S. Geol. Surv. Prof. Pap.* **215**, (1948); P. T. Hayes, *ibid.* **446**, (1964).
2. D. G. Davis, *Natl. Speleological Soc. Bull.* **42**, 42 (1980); S. J. Egemeier, *ibid.* **43**, 31 (1981).
3. D. H. Jagnow, in *Subsurface and Outcrop Examination of the Capitan Shelf Margin, Northern Delaware Basin*, P. M. Harris and G. A. Grover, Eds. (SEPM Core Workshop 13, San Antonio, TX, 1989), p. 459.
4. C. A. Hill, *Geology of Carlsbad Cavern and Other Caves in the Guadalupe Mountains, New Mexico and Texas* (New Mexico Bureau of Mines and Mineral Resources Bulletin 117, Socorro, 1987); C. A. Hill, *Am. Assoc. Pet. Geol. Bull.* **74**, 1685 (1990).
5. J. H. Gardner, *Geol. Soc. Am. Bull.* **46**, 1255 (1935); J. H. Bretz, *J. Geol.* **57**, 447 (1949).
6. D. C. Ford and P. W. Williams, *Karst Geomorphology and Hydrology* (Chapman & Hall, New York, 1992); W. B. White, *Geomorphology and Hydrology of Karst Terrains* (Oxford Univ. Press, New York, 1992).
7. A. N. Palmer, *Geol. Soc. Am. Bull.* **103**, 1 (1991).
8. Spongework mazes (sometimes referred to as boneyard), which exhibit passages resembling the interior of sponge or bone, and ramiform (branching away) passages, types well represented by Carlsbad Cavern and Lechuguilla Cave, are characteristic of hypogene caves (6, 7). Sulfuric acid indicator minerals found in caves of the Guadalupe Mountains include elemental sulfur, gypsum, hydrated halloysite, alunite, natroalunite, jarosite, hydrobasaluminite, and uranyl vanadates; most of these are direct products of cave genesis (2, 4, 10). Light isotopic ratios of sulfur in the cave minerals ($\delta^{34}\text{S} = -30$ to 0 per mil

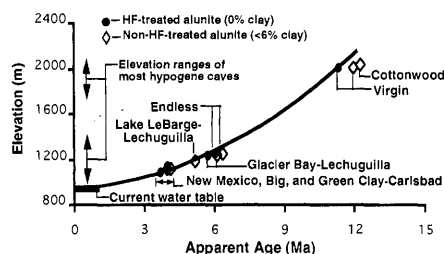


Fig. 5. A plot of apparent ages versus elevation illustrates the strong correlation of elevation with alunite age.

Table 1. Best $^{40}\text{Ar}/^{39}\text{Ar}$ dating results. Ages in boldface (HF-treated samples) represent the most accurate results. Refer to (14) for entire table. Mean crystal sizes and their standard errors were determined by transmission electron microscopy. Clay contamination was estimated by x-ray diffractions.

Cave	Sample	Elevation (m)	Alunite age (Ma)	Crystal size (μm)	Clay (%)
Carlsbad Cavern					
Green Clay Room	30HF	1090	3.89 ± 0.13	1.34 ± 0.05	0
New Mexico Room	29HF	1135	3.98 ± 0.13	1.51 ± 0.05	0
Big Room	28	1115	4.00 ± 0.04	2.02 ± 0.07	3
Big Room	27	1115	4.07 ± 0.07	2.33 ± 0.09	1-5
Endless Cave	02HF	1250	6.02 ± 0.05	1.52 ± 0.08	0
Endless Cave	02	1250	6.34 ± 0.23	1.48 ± 0.04	5
Lechuguilla Cave					
Lake LeBarge	18	1180	5.16 ± 0.13	1.10 ± 0.05	1-5
Glacier Bay	32HF	1230	5.72 ± 0.08	1.29 ± 0.05	0
Glacier Bay	33a	1230	6.07 ± 0.08	1.49 ± 0.07	1-5
Glacier Bay	33b	1230	6.02 ± 0.06	2.88 ± 0.17	3
Glacier Bay	33c	1230	6.02 ± 0.04	8.27 ± 0.50	1
Virgin Cave	20HF	2010	11.30 ± 0.17	2.54 ± 0.16	0
Virgin Cave	20	2010	11.92 ± 0.16	2.58 ± 0.13	5
Virgin Cave	20	2010	12.22 ± 0.16	2.58 ± 0.13	5
Cottonwood Cave	17	2040	12.26 ± 0.16	2.37 ± 0.11	1-5

- relative to troilite in the meteorite Canyon Diablo) indicate that the sulfuric acid responsible for cave genesis was derived from biogenic hydrogen sulfide (4, 9, 10) most likely produced at the base of the Castile Formation in the Delaware Basin immediately south of the Guadalupe Mountains (9). The caves were formed when the hydrogen sulfide was oxidized to sulfuric acid as it migrated upward and approached the water table in the Capitan reef and forereef facies (Capitan Limestone) (9); massive amounts of limestone and dolostone were subsequently dissolved or replaced by gypsum.
9. C. A. Hill, *Geology of the Delaware Basin, Guadalupe, Apache, and Glass Mountains, New Mexico and West Texas*, Permian Basin Section, SEPM Publ. 96-39 (Society for Sedimentary Geology, Tulsa, OK, 1996).
 10. V. J. Polyak and N. Güven, *Clays Clay Mineral.* **44**, 843 (1996); V. J. Polyak and P. Provencio, *J. Caves Karst Studies*, in press.
 11. R. P. Ashley and M. L. Silberman, *Econ. Geol.* **71**, 904 (1976); P. G. Vikre, *ibid.* **80**, 360 (1985).
 12. M. I. Bird, A. R. Chivas, I. McDougall, *ibid.* (*Isotope Geosci. Sect.*), **80**, 133 (1990); G. B. Arehart, S. E. Kesler, J. R. O'Neil, K. A. Foland, *ibid.* **87**, 263 (1992); P. M. Vasconcelos, G. H. Brimhall, T. A. Becker, P. R. Renne, *Geochim. Cosmochim. Acta* **58**, 401 (1994).
 13. D. C. Ford and C. A. Hill, *Isochron/west* **54**, 3 (1989).
 14. Supplementary details of $^{40}\text{Ar}/^{39}\text{Ar}$ analytical procedures, irradiation parameters, and tables of results for individual analyses are available at www.sciencemag.org/feature/data/976753.shl. In summary, samples were irradiated in vacuo with interlaboratory standard Fish Canyon Tuff sanidine as a neutron fluence monitor: FCT-1 with an age of 27.84 Ma [A. Deino and R. Potts, *J. Geophys. Res.* **95**, 8453 (1990)] relative to a Mmhb-1 flux monitor at 520.4 Ma [S. D. Samson and E. C. Alexander, *Chem. Geol. (Isotope Geosci. Sect.)*, **66**, 27 (1987)]. J factors were determined by CO_2 laser-fusion analyses to a precision of ± 0.15 to 0.25% (± 2 sigma). Alunite aliquots (15 to 50 mg) were incrementally heated in a double-vacuum molybdenum resistance furnace in 7 to 10 steps at temperatures of 500° to 750°C . Isotopic compositions of argon were measured with a Mass Analyzer Products model 215-50 mass spectrometer. Decay constants and isotopic abundances used in calculations are those suggested by R. H. Steiger and E. Jäger [*Earth Planet. Sci. Lett.* **36**, 359 (1977)]. Plateau ages and associated uncertainties for samples with flat age spectra, defined by two or more contiguous incremental steps that comprised $>50\%$ of total ^{39}Ar released and agreed in age within 2 standard deviations, were calculated by using the error formula of S. D. Samson and E. C. Alexander [*Chem. Geol. (Isotope Geosci. Sect.)*, **66**, 27 (1987)].
 15. T. C. Onstott, M. L. Miller, R. C. Ewing, G. W. Arnold, D. S. Walsh, *Geochim. Cosmochim. Acta* **59**, 1821 (1995); D. York, N. M. Evenson, P. E. Smith, *U.S. Geol. Surv. Circ.* **1107**, 360 (1994).
 16. R. E. Stoffregen, R. O. Rye, M. D. Wasserman, *Geochim. Cosmochim. Acta* **58**, 917 (1994).
 17. T. Itaya, A. Arribas Jr., T. Okada, *ibid.* **60**, 4525 (1996).
 18. G. E. Hendrickson and R. S. Jones, *Geology and Ground-Water Resources of Eddy County, New Mexico* (New Mexico Bureau of Mines and Mineral Resources Groundwater Report 3, Socorro, NM, 1952); W. S. Motts, *Geol. Soc. Am. Bull.* **79**, 283 (1968); W. L. Hiss, *N.M. Geol. Soc. Guidebook* **31**, 289 (1980); H. R. DuChene and J. S. McLean, in *Subsurface and Outcrop Examination of the Capitan Shelf Margin, Northern Delaware Basin*, P. M. Harris and G. A. Grover, Eds. (SEPM Core Workshop 13, San Antonio, TX, 1989), p. 475.
 19. G. A. Izett, *Geol. Soc. Am. Mem.* **144**, 179 (1975); W. E. Elston, *Tectonics* **3**, 229 (1984); G. P. Eaton in *Continental Extensional Tectonics*, M. P. Coward, J. F. Dewey, P. L. Hancock, Eds. (Geological Society Special Publication 28, Blackwell, Oxford, 1987), p. 355; D. S. Barker, *Geol. Soc. Am. Bull.* **88**, 1421 (1977); J. S. Compton, S. W. Snyder, D. A. Hodell, *Geology* **18**, 1227 (1990); P. Cabezas, *N.M. Geol.* **13**, 25 (1991); C. E. Chapin and S. M. Cather, *Geol. Soc. Am. Spec. Pap.* **291**, 5 (1994).
 20. B. P. Flower and J. P. Kennett, *Palaeogeogr. Palaeoclimatol. Palaeoecol.* **108**, 537 (1994); J. A. Wolfe, *ibid.*, p. 195; C. Latorre, J. Quade, W. C. McIntosh, *Earth Planet. Sci. Lett.* **146**, 83 (1997); G. M. Filippelli, *Geology* **25**, 27 (1997).
 21. We thank C. E. Chapin of the New Mexico Bureau of Mines and Mineral Resources, Socorro, New Mexico; D. C. Ford of McMaster University, Hamilton, Ontario, Canada; and C. A. Hill, consulting geologist, Albuquerque, NM, for their prerreview of this paper.

We thank D. Pate, J. Richards, and the Carlsbad Caverns National Park Service; J. Goodbar and the Carlsbad District Bureau of Land Management; and R. Turner and the Lincoln National Forest Service for the necessary permits and field assistance. Funding for the $^{40}\text{Ar}/^{39}\text{Ar}$ geochronology work was provided by the New Mexico Bureau of Mines and Mineral Resources.

16 December 1997; accepted 5 February 1998

Partial Hormone Resistance in Mice with Disruption of the Steroid Receptor Coactivator-1 (SRC-1) Gene

Jianming Xu, Yuhong Qiu, Francesco J. DeMayo, Sophia Y. Tsai, Ming-Jer Tsai, Bert W. O'Malley*

The in vivo biological function of a steroid receptor coactivator was assessed in mice in which the SRC-1 gene was inactivated by gene targeting. Although in both sexes the homozygous mutants were viable and fertile, target organs such as uterus, prostate, testis, and mammary gland exhibited decreased growth and development in response to steroid hormones. Expression of RNA encoding TIF2, a member of the SRC-1 family, was increased in the SRC-1 null mutant, perhaps compensating partially for the loss of SRC-1 function in target tissues. The results indicate that SRC-1 mediates steroid hormone responses in vivo and that loss of its coactivator function results in partial resistance to hormone.

Sex steroid hormones have central roles in the control of puberty, sexual behavior, and reproductive functions. Their receptors belong to the nuclear receptor superfamily of ligand-dependent transcription factors (1, 2). Upon hormone binding, steroid receptors undergo conformational change, bind to their cognate DNA response elements on nuclear target genes, and recruit coactivators and general transcription factors (GTFs) to form an active transcriptional complex, resulting in site-directed chromatin remodeling and enhancement of target gene expression (1, 3–8). SRC-1 is a coactivator for the steroid receptor superfamily; it functions in transcriptional activation through its histone acetyltransferase activity (HAT) and multiple interactions with agonist-bound receptors, other coactivators such as CBP or P300, other HAT such as p/CAF, and some GTFs such as TBP and TIF1B (7, 9–11). SRC-1 is a member of a gene family that includes SRC-1, TIF2 (also termed GRIP-1 and SRC-2), and p/CIP (also termed RAC3, ACTR, AIB1, and SRC-3) (6, 9–16). Cell-free and in vitro transcription experiments have indicated that the SRC-1 family members enhance receptor-dependent transactivation of nu-

clear genes (6, 9–16). AIB1 is amplified and overexpressed in many breast cancers and thus could have a role in tumorigenesis (16).

To dissect the physiological role of SRC-1 in vivo, we used gene targeting to disrupt the endogenous SRC-1 gene in embryonic stem (ES) cells. The targeting vector contained 3.5-kb (5') and 2.5-kb (3') mouse SRC-1 genomic sequences flanking a GLVP cassette (17) and a neomycin-resistance gene (PGK-neo) (Fig. 1A). In addition, the herpes simplex virus thymidine kinase (HSV-TK) gene was located outside of the SRC-1 sequence and served as a negative drug-selection marker. After correct recombination, the targeting event inserted an in-frame stop codon at the Met³⁸¹ position and deleted ~9 kb of genomic sequence extending downstream of Met³⁸¹. Because the oligonucleotide sequence corresponding to Asp⁸¹⁶ to Thr⁸²⁶ was detected in an Eco RV-Xba I fragment within the 9-kb region, targeting deleted the SRC-1 exon sequence encoding at least 446 amino acids (Met³⁸¹ to Thr⁸²⁶). Except for the NH₂-terminal basic helix-loop-helix and Per-Arnt-Sim (bHLH-PAS) domains, all SRC-1 functional domains for transcriptional activation, HAT activity, and interactions with nuclear receptors CBP, P300, and p/CAF were disrupted by the targeting event (6, 7, 9, 10, 14, 18).

After electroporation and drug selection

Department of Cell Biology, Baylor College of Medicine, Houston, TX 77030, USA.

*To whom correspondence should be addressed. E-mail: berto@bcm.tmc.edu